This paper first appeared in the ninth print edition of *Photovoltaics International* journal.

Fab & Facilities
Materials
Cell Processing
Thin Film
PV Modules
Power Generation
Market Watch

Establishing a reliability methodology for thermal-cycle failure modes for CIGS modules

Kent Whitfield, Tanya Dhir & **Kedar Hardikar**, MiaSolé, Santa Clara, California, USA

ABSTRACT
This paper describes a methodology used to establish reliability of a CIGS thin-film photovoltaic module component based on identification of a failure mode through product thermal-cycling. The initial observation of the failure is described as part of a larger reliability program that progresses from failure mode and effect analysis through a test-to-failure program that has an objective of understanding the ultimate consequence of specific applied stresses on product performance. Once the specific failure mode was discovered, four means of characterizing the mode were applied and are discussed: tensile testing and material analysis, computer modelling, coupon rapid thermal cycling, and mechanical fatigue testing. This work identified the relevant root cause for failure and facilitated a materials change, which itself was subjected to an accelerated testing program to quantify the improvement and determine success of the design. The means of verifying success included meeting an endurance thermal-cycle limit for a collection of samples and subjecting corrected designs to a mechanical fatigue test, where the correlation between thermal cycle and mechanical fatigue were compared using Weibull analysis.

Introduction

Terrestrial field applications of solar photovoltaics have a history that stretches back more than three decades; however, the science required to create a uniform suite of product and component tests that results in the probability of survival over the product service lifetime remains elusive. In the PV industry, these service lifetimes are typically taken to be the manufacturer's warranty, which covers product performance over a span of time that is frequently more than 20 years. It is understood that these warranties are somewhat of a market-driven phenomenon, with most manufacturers adopting their competitor's warranties in order to remain market competitive.

As such, it is natural for some customers to express concern that without a strong reliability methodology, too much emphasis is placed on certification to the PV module qualification standards. In fact, in the absence of a uniform reliability methodology, manufacturers often state that their products exceed multiples of the key stress tests contained in the qualification test standards, yet the question remains of whether or not this is sufficient to claim a reliable product. The top four such qualification test standards (hereafter referred to as the qualification tests) used for product certification are as follows:

- IEC 61215: Crystalline Silicon Terrestrial Photovoltaic (PV) Modules – Design Qualification and Type Approval
- IEC 61646: Thin-Film Terrestrial Photovoltaic (PV) Modules – Design Qualification and Type Approval
- IEC 61730-1, -2: Photovoltaic (PV) Module Safety Qualification
- UL 1703: UL Standard for Safety for Flat-Plate Photovoltaic Modules and Panels.

Osterwald and McMahon provide a detailed history behind the development of the qualification tests, but make a point that successful completion of these tests cannot be misrepresented as predicting service lifetime [1]. Even so, the qualification tests have arguably improved overall PV module field reliability. For instance, a 10-year assessment of PV systems from 1979–1990 indicated a disparaging five-year PV module failure rate of almost 50%, which subsequently dropped to approximately 1.5 failures per 10,000 modules per year with the development of key stress tests, the majority of which remain in the qualification standards [2].

Recent assessments of PV module failure rates in the field are difficult to find in anything other than anecdotal information [3], although Wohlgemuth presents data on the experience of BP Solar that indicates a rate of failure that equates to one module in every 4,200-module years of operation [4].

A key difference between the tests contained in the qualification standards and reliability tests is that the qualification tests were built around the purpose of rapidly detecting known failure or degradation mechanisms [1]. A second difference is that the standard qualification tests contain a definition of failure that all manufacturers' designs must pass in order to enter the marketplace, regardless of design differences and without reference to warranty conditions. As such, these standards cannot assess reliability for unique failure modes that may occur at some point over a particular module's lifetime.

The qualification tests set a minimum expectation for durability or for changes in key performance or safety metrics over time, and contain stress tests such as thermal cycling and damp heat that continue to be indicative of design weaknesses [5]. It is these two key stress tests – thermal cycling and damp heat – that form the basis for a test-to-failure (TTF) program reported by Osterwald and adopted by MiaSolé [6].

Once a TTF program uncovers a failure mode, the reliability engineer's job is to address several key questions:

- What is the root-cause failure?
- What stress or combination of stresses excites the failure?
- Does this stress exist in the field and, if so, to what levels, where, and when?
- Is there a relationship between the level of applied stress and the time to failure?
- Can a process be established to address the root cause and demonstrate that the failure will not occur with unacceptable frequency over the service lifetime?

This paper addresses these questions for an observed failure that occurred at 200% of the standard qualification thermal cycle testing duration.

Failure mode and effect analysis

Failure mode and effect analysis (FMEA) is used to focus resources on those issues deemed by a company to represent an unacceptable risk. A detailed reference on the subject comes from Stamatis [7], but a concise overview is provided by McDermott [8]. FMEA typically takes the form of a design or process review, with a cross-functional team assessing the ways that a part or process could fail to serve its function and the consequences of the identified failure modes. The key outcome of an FMEA is a consensus agreement on how the team's identified risks should be prioritized based on the severity of the failure mode, the probability of its occurrence, and the ability to detect each failure.

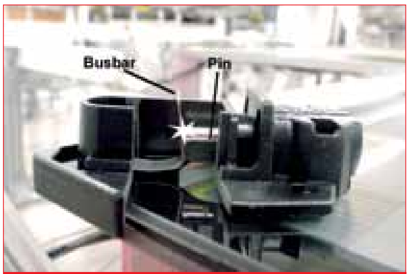

Figure 1. Junction box with a portion of the wall removed to visualize the failure mode of interest.

During the product-design stage, the manner of electrically connecting the PV cells to the junction-box electrical connector pin was evaluated for various failure modes (Fig. 1). Historically, the means of connection between the PV cells and the junction box have exhibited field failures that are attributed to thermal-cycling stress [3, 4, 9].

The failure mode of highest concern was the development of an open circuit having minimal separation distance between the busbar and the junction-box pin connection point that could lead to arcing. The FMEA process concluded that of four different methods of connection (spring clip, screw clamp, soldering, welding), only welding represented the lowest risk for MiaSolé's automated manufacturing process; however, the failure mode itself required testing to better understand its severity.

Failure mode risk assessment

The maximum system voltage of a PV module represents a limit on the number of modules that can be connected together in series, *n*, and can be used to coordinate the voltage insulation ratings for all equipment required in the PV system (cables, fuses, enclosures, inverters, etc.). The number of modules that can be connected in series is determined by local codes or good design practice and is based on the open-circuit voltage, V_{oc}, of the module. Modules delivering maximum power result in an approximate 20% voltage reduction from V_{oc} and at the module level, which is referred to as V_{max}. An arc can be caused by the difference between open-circuit voltage caused by a faulty component and maximum power voltage present during normal operation. At the system level, this voltage is defined as

$$V_x = n^*(V_{oc}-V_{max})$$

The company's FMEA severity assessment used a V_x of 250V DC, which was based on a conservative series connection of modules with a safety margin applied to the voltages. Specially constructed samples were built that could generate a maximum power current arc inside the potted junction box at a voltage that could go as high as 250V. The sample was subjected to repeated internal arc ruptures until oxidation build-up occurred and further arcing was prevented. The outcome suggested that the polymer potting compound did a satisfactory job of containing the arc, but thermal damage to the junction-box enclosure itself was evident. This work was repeated on a second sample with similar results and suggested that the main consequence was thermal damage to the junction box.

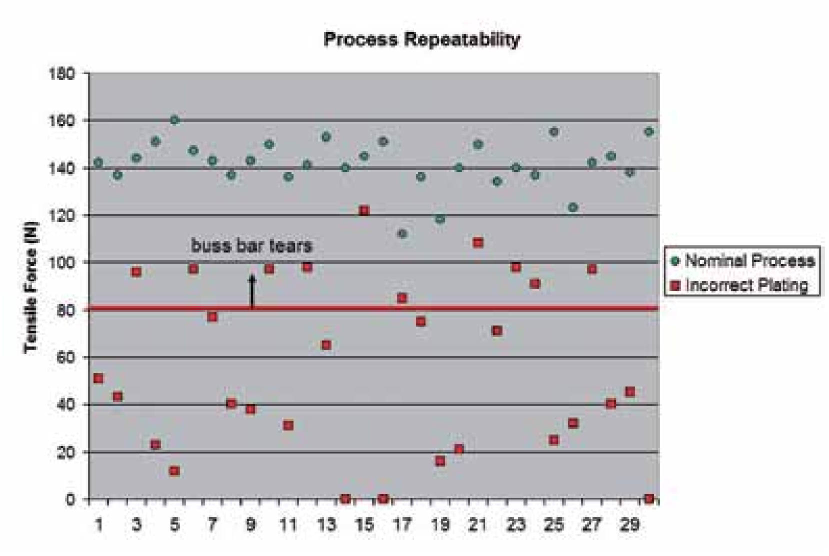

Figure 2. Welded-joint strength repeatability with threshold for busbar tearing identified as red line.

Process development and observation

Based on a clear understanding of the risk, production controls for a fixed combination of pin and busbar materials were developed for the welding method based on a design of experiments (DOE), with key controllable process parameters of current through the joint in amperes, duration of current flow in milliseconds, and clamping pressure on the pieces to be welded in bars.

The key performance metric was the tensile strength of the completed welded joint. Within the process control limitations of ±0.1 bar pressure, ±0.05 amp, ±1 milliseconds, the DOE indicated that current had the largest effect on weld strength and guided the process window to an initial state where repeatability was assessed, as indicated by the nominal process data points in Fig. 2. During process-window development an important demarcation between tensile testing failure modes was observed and is shown in Fig. 2 by a heavy red line. Samples having a tensile strength below this line failed with a clean interface between the pin and busbar. Those failing with a tensile strength above the line always tore the busbar and left busbar material behind on the junction-box pin. This observation became useful in diagnosing a thermal-cycle failure.

Test-to-failure program

Following process development, samples were taken from production and subjected to a TTF program for thermal cycling. (The company's TTF scheme also includes damp heat and humidity freeze testing regimes not discussed here.) The thermal cycle chosen was based on the UL qualification thermal cycle test, which has temperature limits and rate of change of +90°C to -40°C and 120°C/hr, respectively. It should be noted that the IEC qualification standards have an upper temperature limit of 85°C and limit the rate of temperature change to 100°C/hr. Failure was defined as anything constituting a major visual defect according to the qualification standard (i.e., IEC 61646, clause 7) or a maximum power less than 80% of the initial product power (i.e., warranty limit). Detection of the failure and when it occurred was facilitated by running maximum power current through the PV module in a

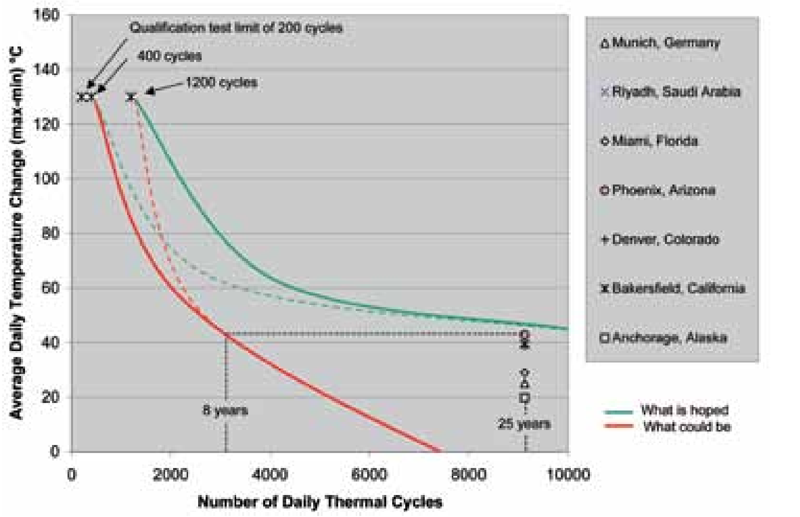

Figure 3. Comparing the qualification thermal cycle to 25-year average daily field thermal cycling.

forward-bias direction and using a data-logger to monitor the current and product temperature throughout the testing duration.

Within six months of initiating the TTF program, several modules had surpassed up to six times the qualification test requirement (1,200 cycles) and were still undergoing testing, but one module had exhibited an open-circuit failure at 400 cycles. Although 400 cycles represents twice the qualification test requirement, it was unclear if this was sufficient for a 25-year product lifetime. The fundamental concern (illustrated in Fig. 3) centres on possible failure curves scenarios as functions of temperature range during the thermal cycle. The chart depicts an estimate of a PV module's average daily field temperature-cycling range for a number of geographical locations and compares it to the qualification temperature change range of 130°C. The field temperature estimate is based on a method for a PV module having a glass-on-glass construction installed in an open rack at an inclination angle equivalent to local latitude and assuming a local 25% ground albedo [10].

> "Although 400 cycles represents twice the qualification test requirement, it was unclear if this was sufficient for a 25-year product lifetime."

When comparing the different temperature change ranges shown in Fig. 3, it is reasonable to expect that the qualification thermal-cycle test will require fewer cycles to cause failure. The problem, however, is that the actual shape of the failure curve remains unknown. To generate such a curve, several different temperature change ranges are required. This quickly becomes a daunting task because even liquid nitrogen-assisted thermal cycling chambers have difficulty exceeding 30 cycles per day because of a module's thermal mass. As such, once a failure is detected, it is typically prudent to develop a faster means to understand the reliability implication based on a clear understanding of root cause and the ability to confirm that an accelerated test appropriately excites the desired failure mode.

Figure 4. View of the junction-box pin following the first occurrence of a failure in thermal cycling.

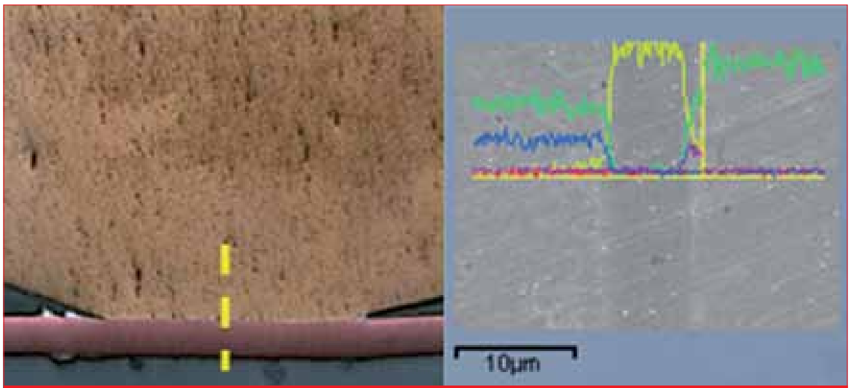

Figure 5a. EDXRS of a polished cross-section of a welded joint from a batch containing an incorrect plating layer which was found in a sample that failed in 400 thermal cycles.

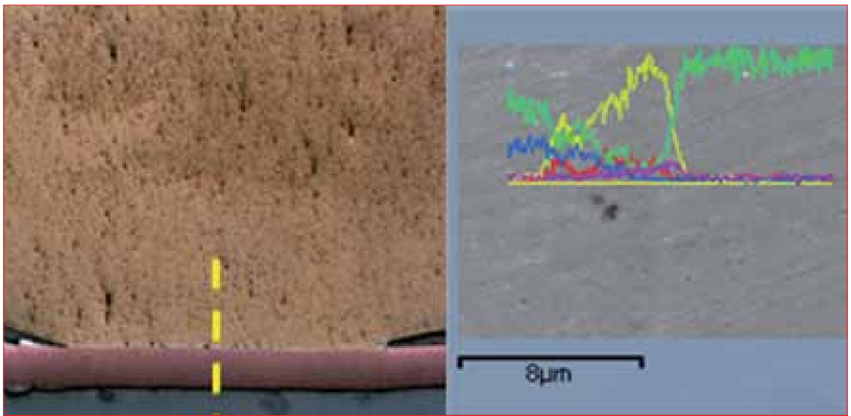

Figure 5b. EDXRS of a polished cross-section of a welded joint from a batch with correct plating layers found in modules that had not exhibited a failure in 1,200 thermal cycles.

Root cause for failure

An autopsy of the module revealed a weld failure between the busbar and the junction-box pin. The busbar itself did not exhibit damage but appeared to be simply separated from the pin. A close examination showed that the original FMEA failure mode of concern was present in the form of arc scoring at the tip of the pin, as depicted in Fig. 4. Note that this arc residue was made visible because the maximum power current was flowing through the module during the test. Although applying current to the module during thermal cycle is not required according to IEC 61646, the technique proved useful in this example of fatigue failure.

Review of the FMEA suggested that a process violation had occurred. It was quickly tied to an incoming material variance in a particular plating layer of the junction-box pin that was confirmed via several methods, two of which – tensile testing and energy dispersive x-ray spectroscopy (EDXRS) – are briefly described in the following sections.

Tensile testing

Tensile testing is an effective means of providing rapid feedback on a fatigue-related failure mode. It has limited value in diagnosing root cause and by itself is insufficient to predict lifetime. However, the speed of its results enables rapid feedback on a DOE test. Computer modelling suggested that the failure mode would be best evaluated by a pull test that placed the weld joint into a combined shear-tensile stress. This method of testing confirmed that a change in weld strength could be tied to lot difference from the part supplier. Consequently, EDXRS allowed identification of a specific layer in the plated pin that was different between incoming lots. Those lots exhibiting low tensile strength additionally showed large piece-to-piece variance in weld strength as the 'Incorrect Plating' data indicate in Fig. 2.

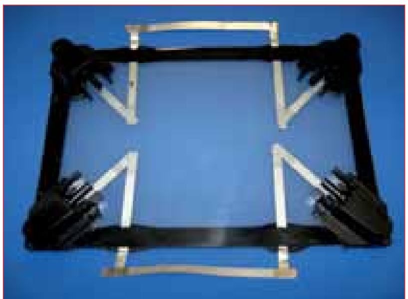

Figure 6. Sample coupons used to understand the nature of the failure.

EDXRS measurements

EDXRS was performed on several cross-sections of welded joints. The measurements allowed visualization of chemical layers involved in the weld and a specific plating layer that limited the degree of metallic mixing taking place at the weld joint (Figs. 5a, 5b). This combination in a mixed metal weld joint (e.g., copper to brass) has been correlated to bond strength. As Fig. 5a illustrates, each elemental layer of the welded joint shows up as a discrete colour trace associated with its chemical identity, while the sharp transitions between the colour traces indicates that very little mixing took place. In Fig. 5b, when the correct plating was present and under the same set of welding conditions as the sample in Fig. 5a, there was a smoother transition from one chemical identity to the next. This smoother transition also correlated with samples that had greater than 80N tensile strength and failed by tearing of the busbar, leaving busbar material at the weld joint.

Reliability analysis

Because the TTF program had resulted in only one failure, little was known about the nature of the failure mode other than that it was linked to incomplete weld penetration. It was, therefore, necessary to understand whether this failure represented either an infant mortality distribution characterized as having a high initial rate of failure with the rate decreasing over time, a random distribution that exhibits relatively constant failure rates over time, or a wear-out failure where the frequency of failures increases over time. It was suspected, and later supported via Weibull analysis, that insufficient weld penetration should lead to an infant mortality failure mode, and that this was a preferred scenario because correct pin plating should improve the joint strength and therefore increase the number of cycles before fatigue failure occurs.

Coupon thermal cycling

Additional thermal-cycling failures were necessary to understand the nature of the failure distribution and to put some context behind the first failure that occurred at 400 cycles. To increase statistics on the failure mode, specially

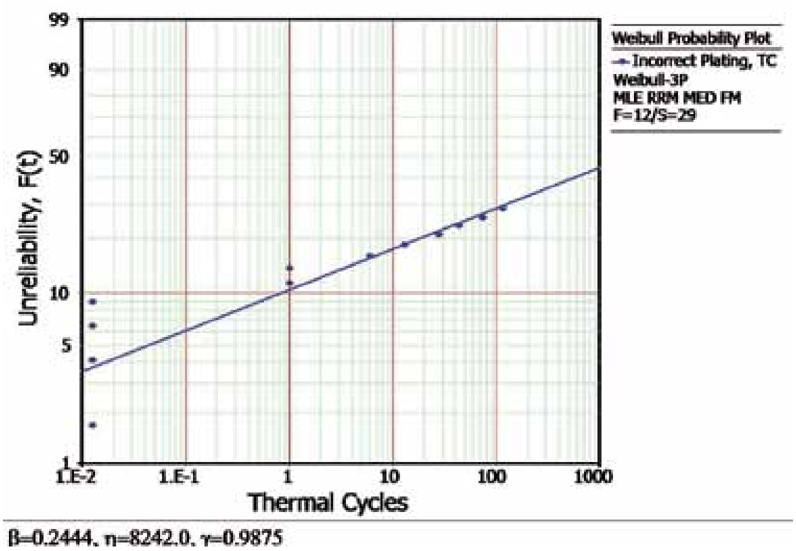

Figure 7. Weibull probability plot for welds from parts anticipated to have low thermal-cycle lifetimes.

constructed samples were made, with four junction boxes each, and current was injected across each weld joint to capture an open-circuit fatigue failure during the thermal-cycle test. The cycles until detection of an open-circuit failure were obtained from a data-logger recording the voltage present across each welded joint. Once 12 failures had been observed within a 200-thermal cycle program, the samples were autopsied to verify that the failure mode was consistent with the originally discovered 400-thermal cycle failure. A Weibull life-data analysis was conducted (see Fig. 7). This analysis is based on the Weibull distribution, which is an extremely flexible frequency distribution that can reproduce positive, normal, or negative distribution skewness and has been used to characterize wide-ranging phenomenon [11], although its use here was strictly to analyze the observed fatigue failures.

The slope of the data in Fig. 7 is referred to as the shape factor, β, which is used to help classify the condition as being either infant mortality, random, or wear-out failure. Given the number of low thermal-cycle failures, β was calculated to be 0.24, which confirmed an infant mortality failure mode – generally the case for β of less than 1. Additionally, the curve indicates that approximately 50% of parts should fail by 1,000 thermal cycles, which put the observed 400 thermal-cycle failure in context. The conclusion was that while some parts may fail at hundreds of thermal cycles, 3.5% of samples will fail at the onset of thermal cycling. In this particular case, the observed 400-thermal cycle failure was clearly unacceptable because of its association with a wide distribution.

Computer modelling

A finite element model (FEM), developed using ABAQUS, was selected to drive understanding of the fatigue failure and to facilitate development of an accelerated testing method [12]. The level of modelling sophistication required depended heavily on objectives set forth. In the case of the junction-box weld, the objectives were to identify the deformation mechanism by which failure of welded joint occurs in thermal cycling, and to enable development of an accelerated test for the joint that can mimic the behaviour in thermal cycling.

“Modelling the system in an elastic-plastic regime was important to understand joint failure through thermal cycling.”

Based on the nominal geometry of the joint, an FEM of half of the junction-box assembly was developed (as depicted in Fig. 8a), with appropriate boundary conditions to represent symmetry. Based on initial calculation, it appeared that modelling the system in an elastic-plastic

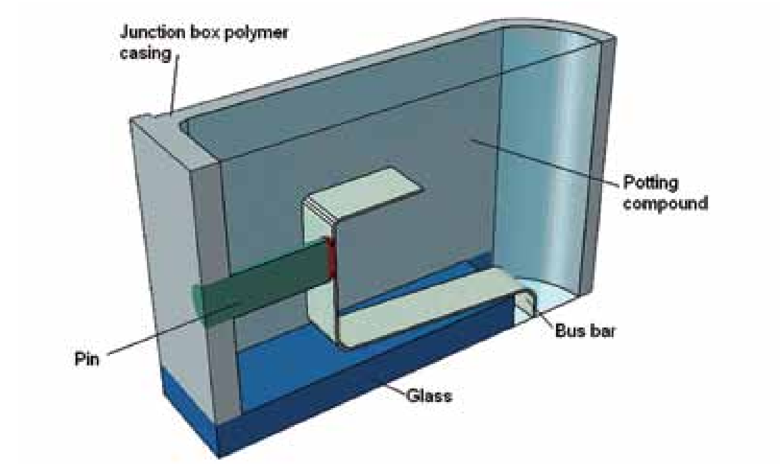

Figure 8a. Simplified geometry used for finite element model.

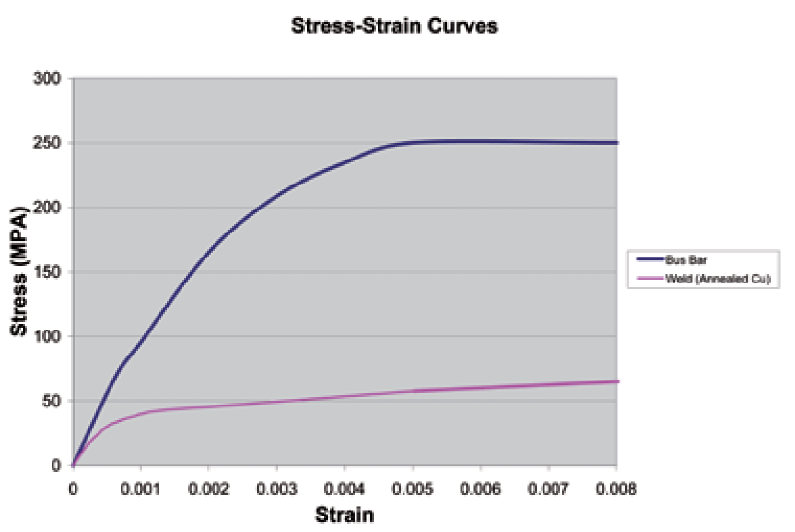

Figure 8b. Stress-strain curves used in the FEM.

Material	Modulus (MPa)	Poisson's Ratio	CTE
Junction-box polymer	2.35×10^3	0.38	7.02×10^{-5}
Busbar (Cu)	1.15×10^5	0.33	1.70×10^{-5}
Junction-box material	9.70×10^4	0.35	1.87×10^{-5}
Glass	7.31×10^4	0.22	9.03×10^{-6}
Potting compound	3.00×10^{-1}	0.45	3.32×10^{-4}

Table 1. Material properties used in analysis.

regime was important to understand joint failure through thermal cycling. Fig. 8b shows stress-strain curves used to model material behaviour for the busbar and weld region [13].

The potting compound that the company selected for its CIGS modules is a highly deformable polymer and the junction box is comparatively rigid. Given the fairly large temperature range of the qualification thermal cycle, it was anticipated that the material characterization would be complex. While dynamic mechanical analysis and other sophisticated techniques are available, it was instead decided to view the system as exhibiting an elastic-perfectly-plastic behaviour. For polymers, the ratio of yield stress to modulus can be as large as 5% [14]. In the present case, significant stress relaxation was anticipated since the loading cycle is slow, and at higher temperatures the material stiffness is expected to be reduced.

The bulk modulus was assumed not to change since the material was considered incompressible. For this study, a representative yield stress was taken to be 1% of the modulus. As the material properties in Table 1 show, the high thermal expansion of the potting compound and elastic-plastic deformations at the welded joint represent key elements for understanding the fatigue behaviour of the welded joint in the thermal cycle.

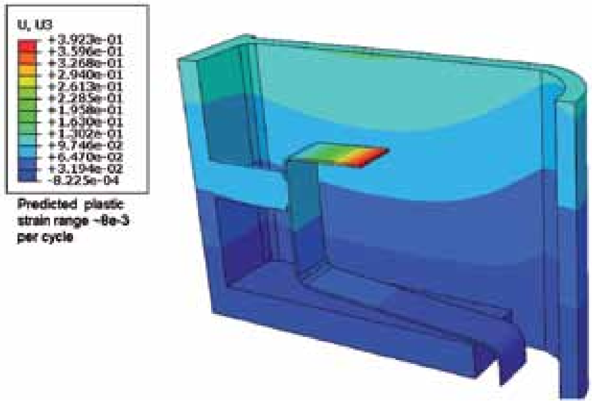

Figure 9a. Mode of deformation predicted by FEM. Note that the folded tab-end of the busbar is the source of stress.

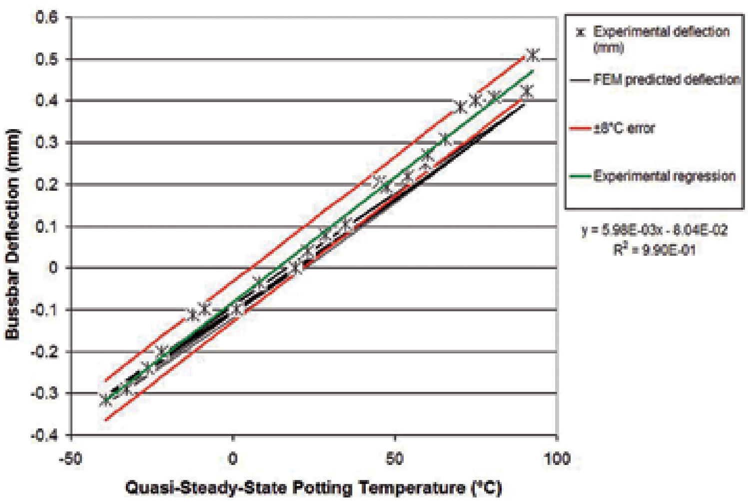

Figure 9b. Comparison of displacements predicted by FEM and experimental measurements described in the text.

Fig. 9a illustrates the mode of deformation from the FEM during thermal cycling and predicted plastic strain at the weld, while Fig. 9b shows a comparison of busbar deflections during thermal cycling predicted by the FEM going through a sequence of 10 cyclic displacements and compared to experiment. The slight change in slope between experiment and model is probably caused by the differences between the actual material used in the product and the material properties assumed for the analysis. Overall, the agreement is considered to be good.

Main insights gained from the FEM are:

- Cyclic deformations of the top bend in the busbar result in high stress/strain amplitude at the welded joint.
- If the welded joint is weaker (due to incomplete penetration), the failure would occur in the joint, whereas in a good joint the plastic strain would propagate in the vicinity of the joint.
- Deformation of the top bend is primarily driven by large expansion and contraction of the potting compound coupled with volumetric constraint offered by junction-box enclosure.

According to the model, the top bent portion of the busbar as well as the geometry of the 'notch' at the welded joint have a large influence on the stress and strain to which the welded joint is subjected.

In principle, FEM-derived calculations can be used to predict fatigue life of the joint by relating plastic strain amplitude to number of cycles to failure using the following relation [15]:

$$\frac{\Delta\varepsilon_p}{2} = \varepsilon_f (2N)^c$$

Where

$\Delta\varepsilon_p$ = Plastic strain amplitude
ε_f = Fatigue ductility coefficient
2N = Number of strain reversals to failure
c = Fatigue ductility exponent

Representative values of $\varepsilon_f = 0.5$, c = -0.6, and $\Delta\varepsilon_p = 8 \times 10^{-3}$ were used to estimate joint life of 3,125 thermal cycles. Although this compared favourably to experimental results, the insights gained from the FEM proved the most useful in developing an accelerated test method.

Accelerated test method

The mechanical fatigue test, guided by the FEM study, had to replicate the actual deflection experienced by the busbar as a function of temperature. A special sample was made to measure the deflection and consisted of a junction box and a small deflection-indicating pin extending up through the potting compound (Fig. 10). The displacement of the pin was measured at various temperatures. The data indicated in Fig. 9b are considered quasi-steady state since the sample had to be removed from an environmental chamber to room temperature conditions to make the measurement. As a result, some noise associated with transient heat-transfer and other uncertainties during the deflection measurement arises, amounting to approximately ±8°C around the regression line.

The Fig. 9b regression equation indicates that a busbar tab (approximately 9mm long) will deflect a total of 0.7mm (±0.35mm) when going from -40°C to +90°C in the thermal cycle test, and this deflection results in a reactionary force at the weld. To conduct a mechanical fatigue test using a reasonable actuator displacement of ±0.5mm at the end of the busbar tab, the weld-reaction force was held constant and used to calculate an equivalent length of busbar required.Special coupons were also created to undergo mechanical fatigue testing. All coupons used unpotted junction boxes that were additionally modified to allow easy access to the end of the busbar tab (Fig. 11). The tab was trimmed to a calculated length, and the mechanical tester was carefully positioned so that the piston would apply the required deflection at the tip. The testing equipment counted the number of cycles applied, and stopped the test whenever electrical continuity between the busbar tip and the junction-box pin was disrupted by an open circuit that might have been indicative of a fatigue failure.

Following the test's completion, each sample was visually examined to note the failure location and specifically check whether or not the failure had occurred at the weld. Some samples with the incorrect plating layer exhibited a second failure mode, consisting of a cracked busbar tab adjacent to the weld. This was a benign failure since it did not affect the electrical continuity of the busbar-to-pin joint and, therefore, would not have affected the power output from a PV module. Examination of the data in Fig. 2 suggests that this finding was consistent with the earlier tensile testing work, because some incorrectly plated parts had welded joints with tensile strengths above 80N – the tensile force required to cause tearing of the busbar material. The large variation of tensile strengths exhibited by the incorrectly plated pin meant that two failure modes should occur and were, in fact, observed.

Figure 10. Coupon prepared to allow busbar deflection measurement as a function of quasi-steady state temperature.

Figure 11. View of fatigue tester with junction box.

The Weibull analysis shown in Fig.12a confirmed that the nature of the mechanically derived failure mode was similar to failures observed in coupon thermal cycling. The result of the analysis indicated consistency between the thermal cycling failures and the mechanical-fatigue failures. This finding is illustrated in Fig. 12b, where the Weibull shape (β) and scale (η) parameters at the 95% confidence level overlap.

The mechanical fatigue testing of

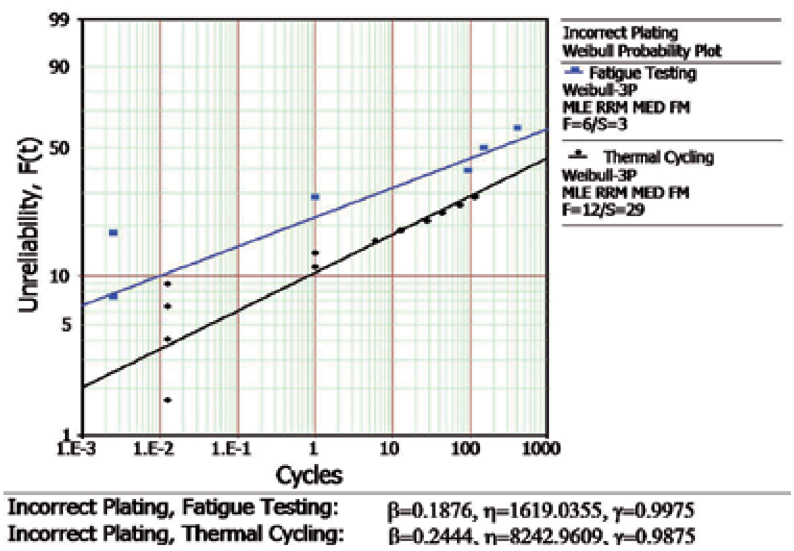

Figure 12a. Comparison between mechanical and thermal-cycle derived failures on a Weibull probability plot.

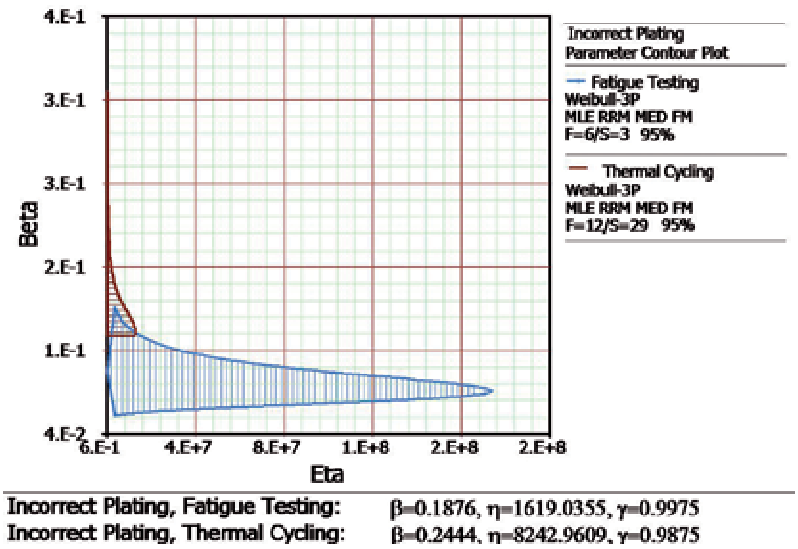

Figure 12b. Mechanical and thermal-cycle derived failures on a Weibull parameter contour plot: overlapping contours indicate they are consistent datasets.

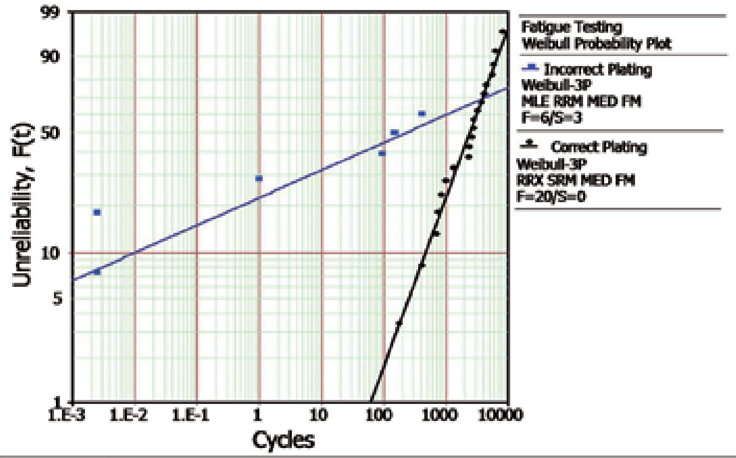

Figure 13. Comparison between infant mortality and benign wear-out failures on a Weibull probability plot.

incorrectly plated parts resulted in a Weibull shape parameter of β of 0.19 that was comparable to the thermal-cycle shape parameter of β of 0.24 and again supported the previous findings that incorrect pin plating created an infant-mortality failure mode. The most important conclusion, however, was that one could stimulate a thermal-cycle fatigue failure mode through mechanical testing. This insight enabled a faster path toward understanding the weld reliability under the aggressive deflection requirements of the qualification thermal-cycle test and eventually supported development of a service lifetime estimation for correctly plated parts that deflect in a manner consistent with anticipated field deflection.

Twenty samples, each with the correct pin plating, were fatigue-tested to failure using deflection based on the qualification thermal-cycle test. The results supported the original hypothesis that pins having the correct plating fostered stronger weld joints that could sustain more fatigue damage before failure. In fact, visual inspection following failure detection indicated that all fails were of the benign type and that none occurred at the weld joint itself. The Weibull probability plot (Fig. 13) also reveals that the nature of the failure has changed from an infant mortality to a wear-out failure where the shape parameter, β, is now greater than 1. A Weibull parameter contour plot for comparing correctly plated pins to incorrectly plated pins was found to be impractical since the parameters were too different from each other to be presented in the same space.

Fig. 13 also shows that the correct plating curve indicates a percentage of parts exhibited benign fatigue failure prior to reaching the 25-year daily cycle limit of 9,125 cycles. Two metrics of interest in defining reliability are the median lifetime and failure-free lifetime. In Weibull analysis the median lifetime represents the centroid of the distribution, and is defined as:

$$B_{50} = \gamma + \eta(\ln 2)^{1/\beta}$$

Where β is the shape, η is the scale parameter previous described, and γ is the location parameter. The median lifetime for correctly plated parts was calculated to be 3,900 cycles, which compares favourably to the FEM prediction of 3,125 cycles. On the other hand, the location parameter, γ has the effect of shifting the failure distribution in time (or in this case, shifting by cycles), and serves as an estimate of the failure-free operating period for the part. For welds made with correctly plated parts, the failure-free operating period is estimated to be 1,468 cycles at the qualification thermal-cycle level and is clearly less than the 25-year daily cycle limit of 9,125.

"Twenty samples, each with the correct pin plating, were fatigue-tested to failure using deflection based on the qualification thermal-cycle test."

The benign failure mode discovered did not pose a safety, performance, or cosmetic risk for warranty return. Thus, it was tempting to avoid testing at smaller deflections that would be more indicative of anticipated field conditions; however, work done to mitigate a specific failure mode inevitably results in slight process changes that, if unstudied, can result in unpleasant surprises.

Service lifetime estimate

To estimate the lifetime of the correct plated pin-to-busbar weld, 10 samples were subjected to an equivalent field cyclic stress condition. Average daily temperature swings for Phoenix, Arizona, were selected based on comparison of several locations (Fig. 14) and converted to an equivalent deflection using the Fig. 9b regression equation. A safety factor of 2 was multiplied to the result to take into account the possibility of more aggressive daily temperature swings elsewhere. Coincidentally, this methodology resulted in a test with 50% of the deflection of the qualification thermal-cycle test.

The results shown in a reliability plot format on Fig. 15 indicate that under service conditions, the initial onset of a benign failure mode (based on location function) occurred at 20,900 cycles, well over the expected service lifetime of 9,125 cycles. This effectively meant that as long as the welding process and material stay within specifications, this failure mode

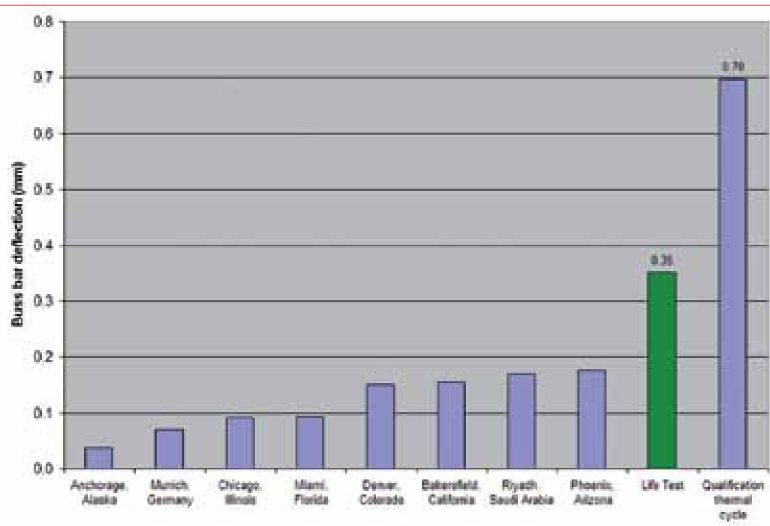

Figure 14. Busbar deflection estimates for various locations with the lifetime test deflection coloured green.

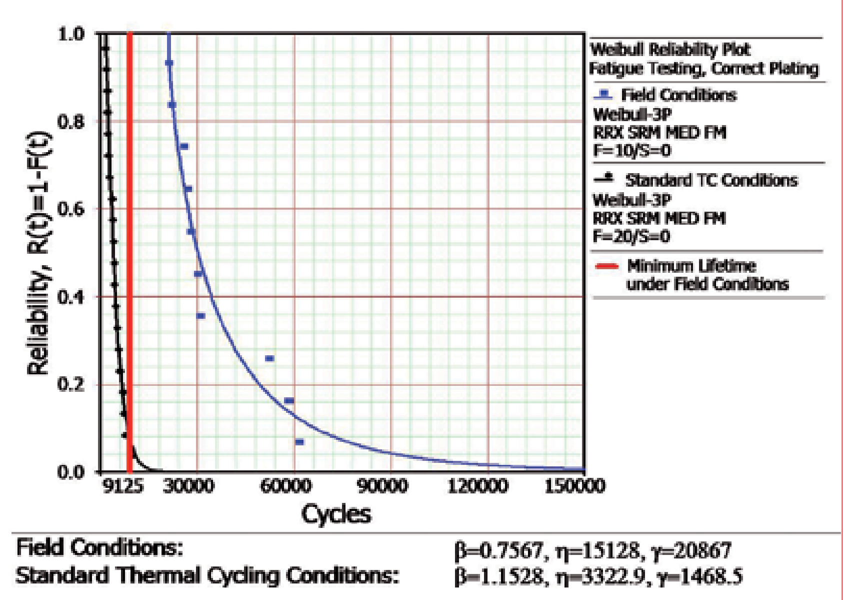

Figure 15. Comparison of fatigue testing results replicating qualification thermal-cycling stresses and anticipated field stresses on a Weibull probability plot.

would not pose a significant warranty risk over a 25-year service lifetime.

Conclusion

The intent of this paper has been to outline a reliability evaluation process used on a specific thermal-cycle failure mode encountered by MiaSolé and because of an absence of general photovoltaic tests that result in a product lifetime estimate. It cannot be concluded that such a process is generally applicable to PV modules, but some principles may be useful in other situations. In this example, the reliability approach began at design and continued through service lifetime estimation for a specific discovered failure mode. Although the work presented here indicated that service lifetime requirements could be met with minimal risk, continued vigilance over the process and additional testing of this failure mode will be required for as long as products with this busbar-to-pin design continue to be deployed.

References

[1] Osterwald, C. & McMahon, T. 2008, "History of Accelerated and Qualification Testing of Terrestrial Photovoltaic Modules: A Literature Review", *Progress in Photovoltaics: Research and Applications*, Vol. 17.

[2] Durand, S. & Bowling, D. 1993, "Field Experience with Photovoltaic Systems: Ten-Year Assessment", Electric Power Research Institute, TR-102138, Final Report.

[3] Laukamp, H. 2002, "Reliability Study of Grid Connected PV Systems, Field Experience and Recommended Design Practice", International Energy Agency, Report IEA-PVPS T7-08:2002.

[4] Wohlgemuth, J. 2003, "Long Term Photovoltaic Module Reliability", NCPV and Solar Program Review Meeting, NREL/CD-520-33586.

[5] Govindasamy, T. et al. 2008, "Failure Analysis of Design Qualification Testing: 2007 vs. 2005", *Photovoltaics International*, Vol. 1.

[6] Osterwald, C. 2008, "Terrestrial Photovoltaic Module Accelerated Test-to-Failure Protocol", National Renewable Energy Laboratory, Technical Report NREL/TP-520-42893.

[7] Stamatis, D. 2003, *Failure Mode Effect Analysis: FMEA from Theory to Execution*, 2nd edition, ASQ Press.

[8] McDermott, R., Mikulak, R. & Beauregard, M. 2009, *The Basics of FMEA*, 2nd edition, Taylor & Francis Group, LLC.

[9] Kurtz, S., Granata, J. & Quintana, M. 2009, "Photovoltaic-Reliability R&D Toward a Solar-Powered World", SPIE Conference, San Diego, California.

[10] Kurtz, S. et al, "Evaluation of High-Temperature Exposure of Photovoltaic Modules", *Progress in Photovoltaics* [in review].

[11] Weibull, W. 1951, "A Statistical Distribution Function of Wide Applicability", *Transactions of the American Society of Mechanical Engineers*.

[12] ABAQUS, v 6.9-EF, Dessault Systems Simulia Corp., Providence, Rhode Island.

[13] *Atlas of Stress-Strain Curves*, 2002, 2nd edition, ASM International.

[14] Ashby, M.F. & Jones, D.R. 1998, *Engineering Materials 2*, 2nd Edition, Butterworth-Heineman, Woburn, Massachusetts.

[15] Dieter, G.E. 1988, *Mechanical Metallurgy*, McGraw-Hill Book Company.

About the Authors

Kent Whitfield is the director of reliability at MiaSolé, where he is responsible for directing PV module and component reliability and certification testing against externally and internally developed criteria. For the past 19 years, he has been involved in all aspects of alternative energy, from testing and certification through manufacture and design. Previously, Whitfield managed the R&D group and Underwriters Laboratories with a focus on PV, fuel cells, and power inverters. He also chaired the UL 1703 and UL 1741 standards, among others, and led the development of uniform certification requirements within the IECEE. A U.S. representative to IEC TC82 WG2 for PV module standards development, Whitfield holds an M.S. in mechanical engineering and is a registered professional engineer.

Tanya Dhir is the senior reliability engineer at MiaSolé, where she is involved in component and final product testing for certification and long-term reliability. She has been involved in various aspects of alternative energy over the past 10 years, and previously, while at Exova, established the first accredited photovoltaic testing lab in Canada. Dhir is on the ASTM E44.09 committee for photovoltaics and is a registered professional engineer.

Kedar Hardikar is a senior scientist at MiaSolé, where his roles include enabling product development and assisting engineering design using computational modelling as a primary tool. While his academic research was focused on development of atomic-scale and nanoscale models for deformations in solids, he has several years of industry experience in computational modelling. Before joining MiaSolé, Kedar worked in the semiconductor capital equipment industry, where he established and managed offshore modelling activity. He received his Ph.D. from Brown University majoring in solid mechanics.

Enquiries

Email: kwhitfield@miasole.com
Tel: +1 650 919 4211